

# The Effect of Different Continuous Cooling Rates on Lattice Constant and Morphology of the $\gamma'$ Precipitates in Nickel-Base Super Alloy Rene 80

Rasoul Salehi Siavashani<sup>1</sup>, A. J. Novinrooz<sup>2\*</sup>, Ali Taherkhani<sup>2</sup>

<sup>1</sup>Advanced Materials Research Center, Faculty of Materials Engineering, Sahand University of Technology, Tabriz, P. O. Box: 51335-1996, Iran.

<sup>2</sup>Department of Physics, Takestan Branch, Islamic Azad University, Takestan, Iran

Received: June 10 2013

Accepted: July 9 2013

## ABSTRACT

Rene 80 is a Nickel- base superalloy which is widely used in gas turbines. In this study, the influence of cooling rate on lattice constant and morphological changes of the  $\gamma'$  precipitates was investigated. The samples were heat treated at 1204 °C for 2 hours, then were cooled to ambient temperature under cooling rates of 0.016, 0.16, 11, 72 and 368 °C/s.  $\gamma'$  precipitates were extracted from the samples by electrolytic method. X-Ray diffraction technique was employed to evaluate the unconstrained lattice constant which was 3.592 Å (=0.3592 nm) for all samples. It has been found that decreasing of the cooling rate from the solution temperature led to changes in the morphology of the  $\gamma'$  precipitates; from spherical to flower-like, octocubic and finally dendritic morphology.

**KEYWORDS:** Rene 80 Ni-base superalloy; the morphology of the  $\gamma'$  precipitates; lattice constant; electrolytic extraction.

## 1. INTRODUCTION

Nickel-base superalloys are used in high temperature performance applications such as gas turbine blades. These alloys possess an excellent high-temperature strength, hot-corrosion resistance and long-term stability [1-3]. Rene 80 is a polycrystalline cast nickel-base superalloy. Strengthening in Rene 80 alloy is provided by the precipitation of coherent  $\gamma'$  phase, an ordered L1<sub>2</sub> phase, in a solid solution of FCC,  $\gamma$  matrix. Rene 80 shows interesting properties at high temperature creep and low cycle fatigue [4-6]. It has been reported that the Rene 80 is used in the temperature range of 760-982°C [7-9]. A number of studies have been carried out on the effect of heat treatment conditions on  $\gamma'$  precipitation in nickel-base superalloys [10-21]. The growth and coarsening of the  $\gamma'$  precipitates happen without any change in lattice constant and chemical composition of the  $\gamma'$  precipitates [19]. The variation of the  $\gamma$ - $\gamma'$  lattice misfit is caused from the chemical composition changes and lattice constant changes of the  $\gamma$  phase [19]. In this case, no experimental reports and coherent studies have been presented. Thus the morphological and unconstrained lattice constant changes were investigated through different solution heat treatments and cooling cycles, in this study.

## 2. MATERIALS AND METHODS

Chemical composition of the Rene 80 is presented in Table 1. Firstly, samples were machined and grounded to obtain 5×5×5 mm cubic. The samples were solution treated at 1204 °C for 2 hours and then were cooled to ambient temperature under different cooling rates. In order to achieve different cooling rates, different media were used such as furnace (0.016, 0.16 °C/s), air (11 °C/s), oil (72 °C/s) and ice brine (368 °C/s). Standard metallographic techniques were used to prepare the samples. There are some useful conventional etchant solutions which are used for metallographic studies of the nickel-base superalloys [12, 19, and 22]. Electro etching with a solution of 23% H<sub>2</sub>SO<sub>4</sub>+ 6% H<sub>3</sub>PO<sub>4</sub>+ 21% HNO<sub>3</sub>+ 50% H<sub>2</sub>O at 2 volts DC current for about 4 seconds was employed. In fact, this etch attacks gamma, the  $\gamma$  matrix phase and  $\gamma'$  particles appear as darker and brighter regions in microstructure, respectively. Microstructure observations were carried out using a Philips XL-30, scanning electron microscope (SEM). Secondary electron detector was used for imaging.

H<sub>2</sub>O-20% vol. H<sub>3</sub>PO<sub>4</sub> was used as the electrolyte to extract the  $\gamma'$  precipitates. Dissolution carried out at 25 °C using 0.18 A/mm<sup>2</sup>. Finally, the  $\gamma'$  precipitates were prepared as the powder samples for XRD analysis. The electrolytic extraction was able to dissolve all the  $\gamma$  phase in the sample [16, 19, 23-28]. The X-ray diffraction (XRD) analysis was carried out by a Philips-PW 1800 diffractometer. All the X-ray scans were performed on the grounded samples between 10 to 100 degrees. The Nelson- Riley method [29] was applied to determine the precise unconstrained lattice constant of the  $\gamma'$  precipitates.

**Table 1.** Chemical composition of Rene 80

| Element | wt. %   |
|---------|---------|
| Ni      | Balance |
| Cr      | 14.06   |
| Co      | 9.49    |
| Mo      | 3.59    |
| W       | 3.84    |
| Ti      | 4.65    |
| Al      | 3.06    |
| Fe      | 0.171   |
| C       | 0.173   |
| Nb      | 0.048   |
| Zr      | 0.043   |
| V       | 0.039   |
| S       | 0.007   |

### 3. RESULTS AND DISCUSSION

Figures 1 to 5 present the microstructure images of the Rene 80 bulk samples under different cooling rates after holding at 1204°C dissolution temperature for 2 h. the precipitates with relatively uniform morphology and distribution were illustrated on the matrix phase  $\gamma$ . By decreasing the cooling rate, the  $\gamma'$  morphology was changed and size of  $\gamma'$  precipitates was increased. the decreasing of cooling rate from 368 °C/s to 0.016 °C/s caused turning the  $\gamma'$  morphology from spherical (Fig. 1) to flower-like (Figures 2 and 3), octocubic (Fig. 4) and finally dendritic morphology (Fig. 5).

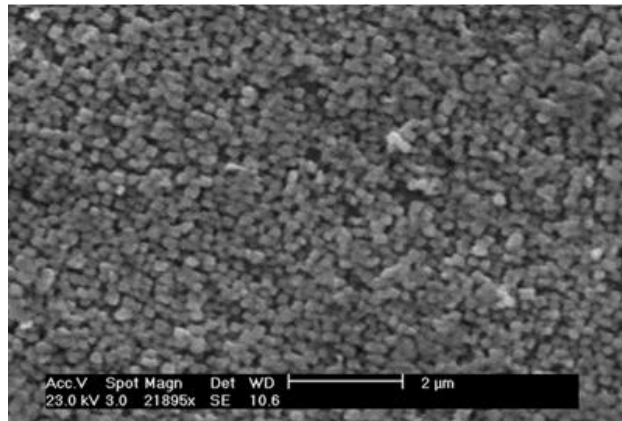


**Fig. 1.** SEM image of the sample subjected to 1204 °C/2 h heat treatment and cooled at 368 °C/s.

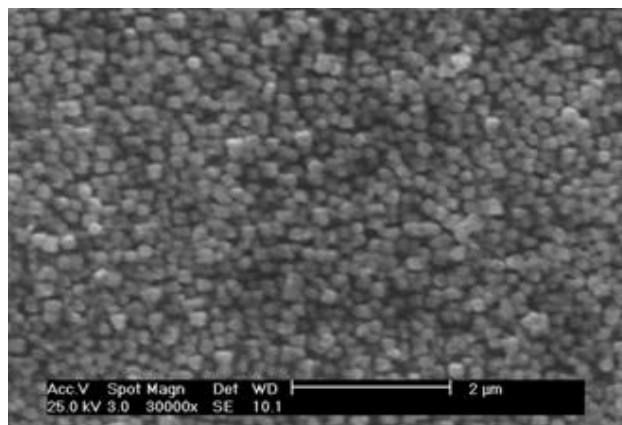


**Fig. 2.** SEM image of the sample subjected to 1204 °C/2 h heat treatment and cooled at 72 °C/s.

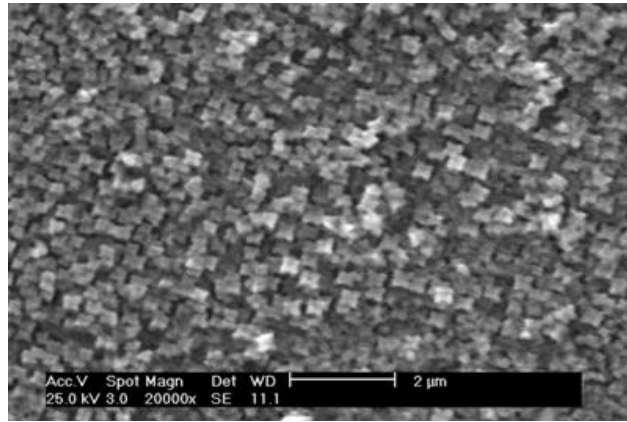


**Fig. 3.** SEM image of the sample subjected to 1204 °C/2 h heat treatment and cooled at 11 °C/s.

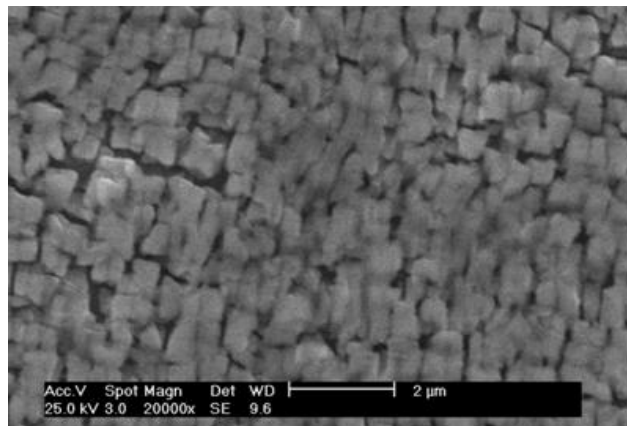


**Fig. 4.** SEM image of the sample subjected to 1204 °C/2 h heat treatment and cooled at 0.16 °C/s.

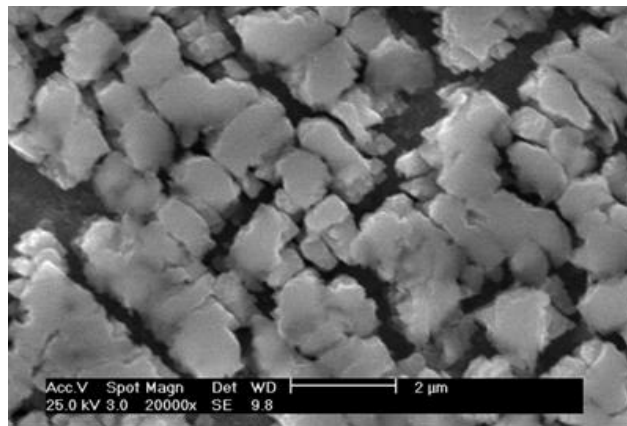


**Fig. 5.** SEM image of the sample subjected to 1204 °C/2 h heat treatment and cooled at 0.016 °C/s.

The dominating rule in the morphology formation of the precipitates is the minimum amount of superficial energy on the interface and the minimum amount of strain energy, resulted from misfit between precipitate/matrix phases, on the precipitate volume unit. If strain energy could be neglected and superficial energy was independent from lattice orientation, the spherical shape would be the preferred morphology. By increasing the misfit between precipitate and matrix phase, strain energy would thoroughly depend on lattice orientation of the precipitate and the spherical shape would not minimize the system's energy anymore [30]. It was believed that  $\gamma'$  precipitates in nickel-base superalloys grow faster in the direction of  $\langle 111 \rangle$  because of more intensive coherence constrains. If the misfit between precipitates and matrix increases, the dominant morphology of  $\gamma'$  precipitates will be spherical, cubic, flower-like, octocubic and

dendritic, respectively [14, 17, and 31]. There are numerous factors which affect on the morphology of  $\gamma'$  precipitates [14, 17, 19, 31-34]; it seems that elastic constrains between the matrix phase  $\gamma$  and precipitate which result from changes of lattice constant of the matrix phase  $\gamma$  is the main factor of these morphology changes [19].

Fig. 6 demonstrates the X-ray diffraction pattern of the  $\gamma'$  powder sample extracted from Rene 80 sample which was rapidly cooled down from the dissolution temperature with the cooling rate of 368°C/s. The lattice constant of the angle was computed by determining the distance of atomic planes in each angle using Bragg's law. Then, Nelson-Riley function was calculated at the given angle (Table 2). Changes of the lattice constant of the angle were plotted in terms of Nelson-Riley function's values, as shown in Fig. 7. According to this diagram, precise lattice constant of each sample was calculated through extrapolation at 90°. This method was used for all the samples and precise lattice constant was computed for all of them; the results are given in Table 3 for all the different cooling rates. The obtained lattice constants of  $\gamma'$  precipitates were almost constant for all the cooling rates, 3.592 Å.

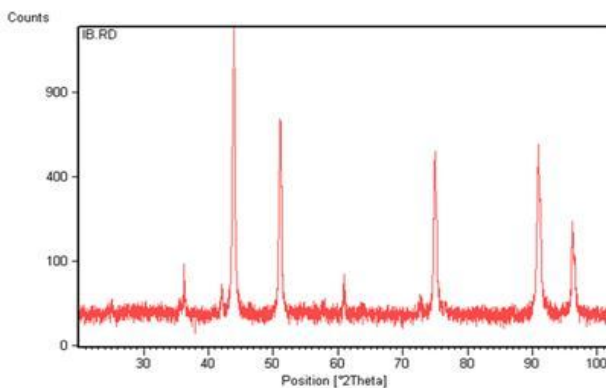


**Fig. 6.** X-ray diffraction pattern of the electrolytic extracted powder of the sample subjected to 1204 °C/2 h heat treatment and cooled at 368°C/s.

**Table 2.** Atomic plane distance, unconstrained lattice constant and Nelson- Riley function for each diffraction peak of the sample subjected to 1204 °C/2 h heat treatment and cooled at 368 °C/s.

| Diffraction angle (2 $\theta$ ) | Atomic plane | d (Å)  | unconstrained lattice constant(Å) | Nelson- Riley function |
|---------------------------------|--------------|--------|-----------------------------------|------------------------|
| 43.91                           | (111)        | 2.0612 | 3.5702                            | 4.5485                 |
| 51.11                           | (200)        | 1.7846 | 3.5729                            | 3.7141                 |
| 74.95                           | (220)        | 1.2666 | 3.5825                            | 2.0000                 |
| 90.91                           | (131)        | 1.0812 | 3.5860                            | 1.3122                 |
| 96.19                           | (222)        | 1.0353 | 3.5866                            | 1.1323                 |

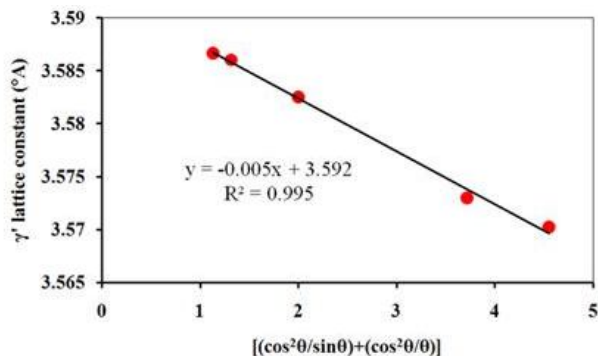


**Fig. 7.** The precise unconstrained lattice constant of the  $\gamma'$  precipitates by means of the Nelson- Riley method for the sample subjected to 1204 °C/2 h heat treatment and cooled at 368 °C/s.

**Table 3.** The precise unconstrained lattice constant of the  $\gamma'$  precipitates under different cooling rates for nickel-base superalloy Rene 80

| Cooling rate (°C/s)                | 368    | 72     | 11     | 0.16   | 0.016  |
|------------------------------------|--------|--------|--------|--------|--------|
| unconstrained lattice constant (Å) | 3.5920 | 3.5920 | 3.5921 | 3.5923 | 3.5923 |

Ardell *et al.* [35] assumed that  $\gamma'$  precipitates have constant chemical composition. They explained that the matrix around the coherent  $\gamma'$  precipitates was richer in alloying elements in comparison to non-coherent  $\gamma'$  precipitates. So, it can be expected that lattice constant of the matrix phase would change by chemical composition, but chemical

composition and lattice constant of  $\gamma'$  precipitates remain constant. However, applying elastic constrain from the matrix phase  $\gamma$  to  $\gamma'$  precipitates changes the results obtained from  $\gamma'$  precipitates' lattice constants in the bulk form [19]. Based on these conditions, it can be stated that the unconstrained lattice constant of  $\gamma'$  precipitates would be constant in different morphologies. morphological changes would be due to the change of matrix phase's lattice constant and applying elastic constrain from the matrix phase on  $\gamma'$  precipitates under the bulk form, not due to the changes of chemical composition and unconstrained lattice constant of  $\gamma'$  precipitates [19, 35].

#### 4. CONCLUSION

In this study, morphological changes of  $\gamma'$  precipitate in superalloy Rene 80 were reported during cooling from dissolution temperature. The precipitates were turned from spherical to flower-like, octocubic and finally dendritic with the decrease of cooling rate. The precise unconstrained lattice constant of  $\gamma'$  precipitates was constant in different morphologies and it was 3.592 Å. The morphological changes of precipitates were caused by elastic constrains between matrix phase and precipitate in bulk form while unconstrained lattice constant of  $\gamma'$  precipitates was constant.

#### REFERENCES

1. Donachie, M.J., S.J. Donachie, 2002. Superalloys, A technical guide. Materials Park (OH), ASM International, 18-35.
2. Durand-Charre, M., 1997. The Microstructure of Superalloys, Amsterdam. Gordon and Breach Science Publishers, 32-50.
3. Sims, C.T., N.S. Stoloff, W.C. Hagel, 1987. Superalloy II. New York, Wiley, 45-60.
4. Rahmani, K., S. Nategh, 2008. Low cycle fatigue mechanism of Rene 80 at high temperature–high strain, *Mat. Sci. Eng. A*, 494. 385-395.
5. General Electric Specification no. GE C50 TF28, Rene-80 investment vacuum cast turbine blades and vanes, 1976.
6. Safari, J., S. Nategh, 2009. Microstructure evolution and its influence on deformation mechanisms during high temperature creep of a nickel base superalloy, *Mat. Sci. Eng., A*, 499: 445-450.
7. Neidel, A., S. Riesenbeck, T Ullrich, J Volker and Yao, 2005. Hot cracking in the HAZ of laser-drilled turbine blades made from Rene 80, *Materialpruefung/Mat. Test*, 47: 553-560.
8. Domas, P.A., S.D. Antolovich, 1985. A mechanistically based model for high temperature notched LCF of rene 80, *Eng. Fract. Mech.*, 21, 203-210.
9. Goswami, T., 2001. H. Hanninen: Dwell effects on high temperature fatigue damage mechanisms: Part II, *Mat. Des.*, 22: 217-225.
10. El-Bagoury, N., M. Waly, A. Nofal, 2008. Effect of various heat treatment conditions on microstructure of cast polycrystalline IN738LC alloy, *Mat. Sci. Eng. A*, 487: 152-160.
11. Balikci, E., R. A. Mirshams, A. Raman, 1999. Microstructure evolution in polycrystalline IN738LC in the range 1120 to 1250, *Z Metallkd*, 90: 132-140.
12. Behrouzghaemi, S., R.J. Mitchell, 2008. Morphological changes of  $\gamma'$  precipitates in superalloy IN738LC at various cooling rates, *Mat. Sci. Eng. A*, 498: 266-275.
13. Furrer, D.U., H.J. Fecht, 1999.  $\gamma'$  Formation in Superalloy U720LI, *Scripta Mat.*, 40: 1215-1225.
14. Grosdidier, T., A. Hazotte, A. Simon, 1998. Precipitation and dissolution processes in  $\gamma/\gamma'$  single crystal nickel-based superalloys, *Mat. Sci. Eng. A*, 256: 183-188.
15. Monajati, H., M. Jahazi, R. Bahrami, S. Yue, 2004. The influence of heat treatment conditions on  $\gamma'$  characteristics in Udimet 720. *Mat. Sci. Eng. A*, 373: 286-293.
16. Mitchell, R.J., M. Preuss, M.C. Hardy, S. Tin, 2006. Influence of composition and cooling rate on constrained and unconstrained lattice parameters in advanced polycrystalline nickel– base superalloys, *Mat. Sci. Eng. A*, 423: 282-291.

17. Ricks, R.A., A.J. Porter, R.C. Ecob, 1983. The Growth of  $\gamma'$  Precipitates in Nickle-base Superalloys, *Acta Met.*, 31: 43-56.
18. Sajjadi, S.A., H.R. Elahifar, H. Farhangi, 2008. Effects of cooling rate on the microstructure and mechanical properties of the Ni-base superalloy UDIMET 500, *J. Alloys Comp.* 455: 215-226.
19. Savadkoohi, M.K., A. Samadi, R. Salehi, 2011. Cooling rate dependent morphology of the  $\gamma'$  precipitates in nickel-base superally Udimet 500, *Adv. Mat. Res.*, 278: 108-115.
20. Moshtaghin, R.S., S. Asgari, 2003. Growth kinetics of  $\gamma'$  precipitates in superalloy IN-738LC during long term aging, *Mat. Des.*, 24: 325-334.
21. Steven, R.A., P.E.J. Flewitt, 1978. Microstructural changes which occur during isochronal heat treatment of the nickel-base superalloy IN-738, *J. Mat. Sci.*, 13: 367-374.
22. Vander Voort ,G.F. , 1984. *Metallography, Principles and Practice*. New York, McGraw-Hill, pp: 450-460.
23. Kriege O.H., 1974. Phase separation as a technique for the characterization of superalloys, *Metallography-A practical tool for correlating the structure and properties of materials*, ASTM STP, 557: 220-231.
24. Kriege, O.H, J.M. Baris, 1969. The chemical partitioning of elements in Gamma Prime separated from precipitation-hardened, high- temperature nickel-base alloys, *Trans. ASM*, 62: 195-203.
25. Moshtaghin, R.S., S. Asgari, 2004. The influence of thermal exposure on the  $\gamma'$  precipitates characteristics and tensile behavior superalloy IN-738LC, *J. Mat. Proc. Tech.*, 147: 343-352.
26. Moshtaghin, R.S., S. Asgari, 2004. The effect of thermal exposure on the  $\gamma'$  characteristics in a Ni- base superalloy, *J. Alloys Comp.*, 368: 144-152.
27. Penkalla, H.J., A. Czyrska-Filemonowicz, 2003. Quantitative microstructural characterization of Ni-base superalloys, *Mat. Chem. Phys.*, 81: 417-425.
28. Soleimani, S., A. Abdolah-Zadeh, A. Samadi, H. Assadi, 2007. A study of growth kinetics and distribution of  $\gamma'$  precipitates in an induction-aged nickel-base superalloy, *J. Optoelec. Adv. Mat.*, 9: 1789-1795.
29. Cullity, B.D., 1978. *Elements of X-ray Diffraction*. Massachusetts, Addison-Wesley Pub. Co., pp: 600-630.
30. Brooks, C.R., 1982. *Heat Treatment, Structure, and Properties of Nonferrous Alloys*, American Society for Metals, pp: 380-430.
31. Yoo, Y.S., D.Y. Yoon, M.F. Henry, 1995. The effect of elastic misfit strain on the morphological evolution of  $\gamma'$  precipitates in a model Ni-base superalloy, *Met. Mat.*, 1: 47-55.
32. Khachatryan, A.G., S.V. Semenovskaya, J.W. Morris, 1988. Theoretical analysis of strain-induced shape changes in cubic precipitates during coarsening, *Acta Met.*, 36: 1563-1570.
33. Yoo, Y.S. , 2005. Morphological instability of spherical  $\gamma'$  precipitates in a nickel base Superalloy, *Scripta Mat.*, 53: 81-88.
34. Yeom, S.J., D.Y. Yoon and M.F. Henry, 1993. The morphological changes of  $\gamma'$  precipitates in a Ni-8Al (wt pct) alloy during their coarsening, *Met. Tra. A*, 24: 1975-1981.
35. Li, F., A.J. Ardell, 1998. The incoherent  $\gamma/\gamma'$  solvus in Ni-Al alloys, *J. Phase Equ.*, 19: 334-341.